Reports in Mechanical Engineering
Vol. 7, No. 2, 2026, pp. 44-66
ISSN: 2683-5894, DOI: https://doi.org/10.5281/zenodo.21910721

Mechanical Performance Enhancement of EPDM Rubber Nanocomposites Reinforced with Graphene, Carbon Nanotubes, and Silica for Industrial Diaphragm Applications

Al-Hadrayi Ziadoon M. R.[1]*, Hayder H. Khaleel[2], Ammar R. Hasan[3], Emad Kadum Njim[4]
[1] Mechanical Engineering Department, Faculty of Engineering, University of Kufa, Najaf, Iraq
[2] Engineering Technical College, Najaf, Al-Furat Al-Awsat Technical University, Al-Najaf 31001, Iraq
[3] Materials Engineering Department, Faculty of Engineering, University of Kufa, Najaf, Iraq
[4] Department of Mechanical Power Engineering, College of Technical Engineering, University of Al Maarif, Al Anbar, Iraq

Article Info

Article history:

Received April 2, 2026
Revised April 17, 2026
Accepted May 21, 2026

Keywords:

Rubber Composites,
EPDM,
Experimental Tests,
Nanoparticles,
Mechanical Properties

ABSTRACT

Ethylene propylene diene monomer, or EPDM, is a rubber used in several industrial applications. In pipes for sealing water or for rotating equipment, the same can be said of thermal and electrical insulation. EPDM is not only tough and adaptable but also has many applications. Natural sunlight and ozone both harm it, making it brittle over time, but some rubbers, like EPDM, are made for toughness and can withstand a variety of harsh situations. EPDM rubber composites reinforced with three different kinds of reinforcement nanoparticles are employed in the manufacturing of rubber diaphragms. The combined use of analytical, numerical, and statistical methods provides a comprehensive framework for predicting and validating the mechanical performance of EPDM nanocomposites. Based on this, the estimated mechanical properties of Graphene nanoparticles yielded higher values than those of carbon nanotubes and Silica nanoparticles, respectively. Moreover, both CNT and Graphene showed the maximum tensile modulus, impact strength, and fatigue life, while the tensile modulus at 5 wt% increased from 3.5 MPa to above 7 MPa. The coefficient of determination (R^2) values remain close to unity, providing strong evidence of a positive correlation between experimental measurements and model predictions. This confirms that the model successfully captures the underlying material behavior and the influence of nanofiller content.

Corresponding Author:

Al-Hadrayi Ziadoon M. R.
Mechanical Engineering Department, Faculty of Engineering, University of Kufa, Najaf, Iraq
Email: zaidoonm.rahi@uokufa.edu.iq

1. Introduction

Ethylene Propylene Diene Monomer (EPDM) rubber is used in industry for its excellent resistance to heat, weather, ozone, and ageing. However, to improve the material's mechanical performance for more demanding applications, such as automotive seals, vibration dampers, and industrial gaskets, researchers are developing novel possibilities to use nanomaterials for reinforcement. Nano-based materials (such as graphene, carbon nanotubes (CNTs), nano-silica, and nano-clay) have the potential to enhance EPDM composites' stiffness, durability, and fatigue resistance through high surface area and exceptional mechanical properties. Also, due to the acceleration of technology in materials science and engineering, such as functionally graded materials manufactured from polymeric materials, whether of two different types or with metals and ceramic materials, to improve mechanical properties and vibration properties and the use of numerical methods in this field (Khaleel & Al-Hadrayi, 2025). Recent studies have demonstrated that EPDM composites reinforced with nano-fillers exhibit significant improvements in tensile strength, compression resistance, and thermal stability (Cui et al., 2024; Sumbodo et al., 2025). Despite this, challenges remain in achieving uniform dispersion and understanding long-term performance under cyclic loading. This study proposes a novel experimental and computational approach to analyze the mechanical behaviour of nanoparticle-reinforced EPDM rubber composites for industrial applications. Amani et al. (2025) completed the enhancement of mechanical properties in ethylene propylene diene monomer/natural rubber nanocomposites through Ti_3C_2TX reinforcement and EPDM-g-MAH compatibilization. Moreover, Simet et al. (2023) investigated the ageing behaviour of ethylene-propylene-diene monomer (EPDM) in a PMDI environment using surface NMR. Hou et al. (2025) predicted viscoelastic behaviour and crack propagation in EPDM rubber under long-term thermal ageing. However, Bingöl et al. (2025) investigated the properties of mesoporous SiO2-filled EPDM (ethylene-propylene-diene monomer).

Rubber. Azizli et al. (2020) examined the compatibility, mechanical, and rheological properties of hybrid rubber NR/EPDM-g-MA/EPDM/graphene oxide nanocomposites: Theoretical and experimental analyses. de Souza et al. (2025) conducted experimental and numerical studies of thermo-oxidative ageing in NBR and EPDM rubber with varying lengths. Cui et al. (2024) examined evidence for non-Arrhenius behaviour of EPDM rubber by combining Arrhenius and time–temperature superposition (TTS) extrapolations. J. Xu et al. (2025) combined the application of synergists from bittern and bio-based multifunctional modifiers to EPDM rubber composites, focusing on processing, fire safety, mechanical, and anti-ageing properties.

Eyssa et al. (2024) used the neutron attenuation performance of EPDM rubber with BN Nanoparticles/B2O3 composite and studied physical, thermal, and mechanical properties. Du et al. (2025) reviewed ceramizable EPDM composites, including current status and future perspectives. Khozemy et al. (2024) completed a comparative study of the mechanical and thermal properties of EPDM rubber/cement kiln dust composite cured by ionizing radiation. Fang et al. (2025) prepared polysiloxane-functionalized polyolefin with unsaturated groups to improve the compatibility of EPDM/silicone rubber blends. Burgoa et al. (2024) completed rheology as a powerful help for the characterization of the morphology of thermoplastic elastomers (TPE) based on PP and reclaimed EPDM rubber. Wang et al. (2025) investigated the microstructure, mechanical properties, and thermal degradation kinetics of EPDM under thermo-stress conditions used for joint sealing of a floating prefabricated concrete platform for offshore wind power. Lee et al. (2019) used rubber compounds made of modified ethylene propylene diene monomer (EPDM) for laminated bearings with excellent anti-peel strength. Colom et al. (2024) examined the recycling of devulcanized EPDM to improve the engineering properties of SBR rubber compounds.

Wang et al. (2024) examined the simultaneous achievement of excellent heat ageing resistance and grip performance in carbon black/glass flake/EPDM rubber composites for overhead line spacers. Vishvanathperumal and Anand (2021) employed nanosilica-reinforced EPDM silicone rubber blends by using experimental and theoretical evaluation of mechanical and solvent sorption properties. Ling et al. (2025) utilized high mechanical interlocking and hydrogen bonding-based carboxymethyl cellulose/SiO2 composite structures for the interfacial bonding of reinforced polyimide fibre/EPDM composites. Luo et al. (2025) investigated the recycling of EPDM rubber via thermomechanical devulcanization, including both batch and continuous operations. Yu et al. (2025) used in situ grafted ethylene propylene diene monomer (EPDM) rubber multiblock copolymers as compatibilizers for polyethene (PE) and isotactic polypropylene (iPP) blends. Gong et al. (2024) estimated the time-varying compressive properties and constitutive model of EPDM rubber materials for tunnel gasketed joints. Hayeemasae and Ismail (2023) completed an investigation on the viscoelastic behaviour of virgin EPDM/ reclaimed rubber blends using the Generalised Maxwell Model (GMM). Zhang et al. (2021) used theoretical and experimental characterization to study the macro-micro friction behaviours of EPDM rubber. In the same manner, Kiran et al. (2023) conducted an experimental study of vibration attenuation at rail joints by using Ethylene Propylene Diene Monomer (EPDM) rubber. Later, Spanheimer et al. (2025) checked the Ageing behaviour and molecular/network structure evolution of EPDM/carbon black composites under compression and in thermal-oxidative environments.

Akrami and Park (2024) presented advanced polycarbonate foam: Enhancing foamability and mechanical properties with toughened polycarbonate using the nanofibrillation method and crosslinked rubbery EPDM networks. Additionally, Moustafa et al. (2020) investigated the impact of green modification of nanoclay on the adhesion behaviour of EPDM rubber to polyester fabric. Xu et al. (2019) investigated the effects of crosslinked rubber particles on the rheological behaviour of ethylene-propylene-diene rubber/polypropylene thermoplastic vulcanizates. M. Xu et al. (2025) included a type of shape memory material based on ethylene-propylene-diene rubber (EPDM)/ polypropylene (PP) thermoplastic vulcanizates compatibilized by magnesium maleate. Li and Gong (2024) investigated compressive stress-thermo-oxidative ageing behaviour and mechanism of EPDM rubber gaskets for sealing resilience assessment. Wang et al. (2023) explored the effect of aramid and carbon fibers with nano carbon particles on the mechanical properties of EPDM rubber thermal insulators for solid rocket motor applications. Recently, numerous studies have investigated the effects of reinforcing materials on the stability and performance of EPDM rubber composite structures (Foltuț et al., 2025; Gupta et al., 2025; Ndour et al., 2025). Mukhopadhyay and Roy (2023) presented a detailed study on the abrasive wear pattern of ethylene propylene diene monomer (EPDM) rubber compound. Also, Marin-Genesca et al. (2023) completed an evaluation and rationale of the performance of several elastomeric composites incorporating devulcanized EPDM. Spencer et al. (2020) investigated experimental and simulation studies of degraded EPDM composite in coupled gamma radiation-thermal environments. In addition to that, Prut et al. (2017) investigated the rheological behaviors of blends based on polypropylene and EPDM rubber powder. Foltuț et al. (2025) checked the effect of load on the stick-slip phenomenon and wear behavior of EPDM. The most popular uses of EPDM rubber composites are automotive EPDM Sealing and Vibration Damping Systems and diaphragms. Examples of EPDM Diaphragm Applications: Brake booster diaphragms, Pneumatic control valves, Industrial pumps and regulators, Fuel system diaphragms, Air suspension systems. These often require: Thin-section, high-fatigue rubber, Low permanent set, Resistance to aggressive fluids (Triganza et al., 2025).

This research synthesises and characterises EPDM composite diaphragms reinforced with different types and concentrations of nanoparticles (e.g., graphene, nano-silica, and CNTs) for use in manufacturing industrial rubber parts. The mechanical profile of rubber composite samples was assessed: bending, compression, impact, and fatigue. This research also involved constructing a MATLAB-based modelling tool to predict these properties from the input parameters (filler type, weight %, and geometrical conditions) and to compare the experimental and simulated data for model validation. Finally, the proposed analytical methods such as experimental testing, analytical modeling, and FEM simulation are employed to predict the material behavior and to optimise the diaphragm design for industrial application.

This paper is organized into five sections. This study methodology is described in section two. Section 3 presents experimental details. The fourth section presents numerical examples along with compression, bending, impact, and fatigue test results on EPDM-Nano-filler samples. Section 5 concludes the present work with practical suggestions for future work.

2. Methodology

In this work, three complementary approaches, analytical modelling, finite element modelling (FEM) and statistical evaluation, were used to achieve a comprehensive understanding of the mechanical behaviour of EPDM nanocomposites. Each method has its own purpose in the prediction, simulation and validation of material performance. The overall results of combined R2 and RMSE confirm the robustness, reliability and practical applicability of the proposed modelling approach.

In this work, a base polymer matrix, EPDM, with carbon Black (N330) as a primary reinforcing filler, and three types of nanoparticles as secondary filler reinforcement, is used to construct rubber composites. A paraffinic oil (plasticiser, Flexibility, processability), Zinc Oxide (ZnO) used as an activator for sulfur vulcanisation, and stearic acid as a co-activator for ZnO in the mixing process are used. In addition to that, many chemicals are used to Form compounds, including sulfur as a crosslinking agent and accelerator (e.g., CBS or TBBS) for vulcanization, and antioxidants (e.g., TMQ, 6PPD) for thermal/oxidative stability. This research adopted a laboratory experimental methodology that included the following:

Our research methodology involves several key steps. First, we prepare the materials by blending the EPDM matrix with varying concentrations (0 to 5 wt%) of nanoparticles. We then conduct experimental testing according to the ASTM-compliant tests for bending (D790), compression (D575), impact (D256), and fatigue (D3479). These tests are crucial in evaluating the performance of the rubber diaphragm samples in pneumatic and thermal systems. Finally, we complete the computational analysis using a MATLAB-based model, employing regression or machine learning to estimate properties based on composition and testing parameters .

EPDM is currently considered a standard material for industrial and automotive diaphragms, characterised by excellent heat and ozone resistance, flexibility at low temperatures, good dynamic fatigue and chemical resistance, and is one of the base raw materials for industrial and automobile diaphragms. Nevertheless, we aim to further advance the use of EPDM by reinforcing it with nanoparticles to enhance its strength. Such treatment might optimise important diaphragm properties, thereby improving the performance of EPDM for diversified applications.

3. Materials and Methods

EPDM is a very weather-resistant, flexible, and chemically inert rubber suitable for outdoor, sealing, and insulation applications. For its mechanical characteristics, it normally has moderate to good performance depending on the compounding grade. Nanosilica is a stronger, more efficient approach for mechanical strengthening with a simpler processing and manipulation procedure than the others, and offers enhanced stiffness, tensile properties and weatherability. Graphene contributes moderate mechanical and dielectric enhancements, while having better dispersion compared to CNTs. It improves dielectric strength, barrier properties, and thermal conductivity. (Fang et al., 2025; Sharma et al., 2026). Furthermore, CNTs provide superior mechanical stiffness and electrical/thermal conductivity enhancements, but they are more challenging to disperse and may reduce ductility at higher loadings. However, the materials used in this study were all obtained in their original state, including various reagents.

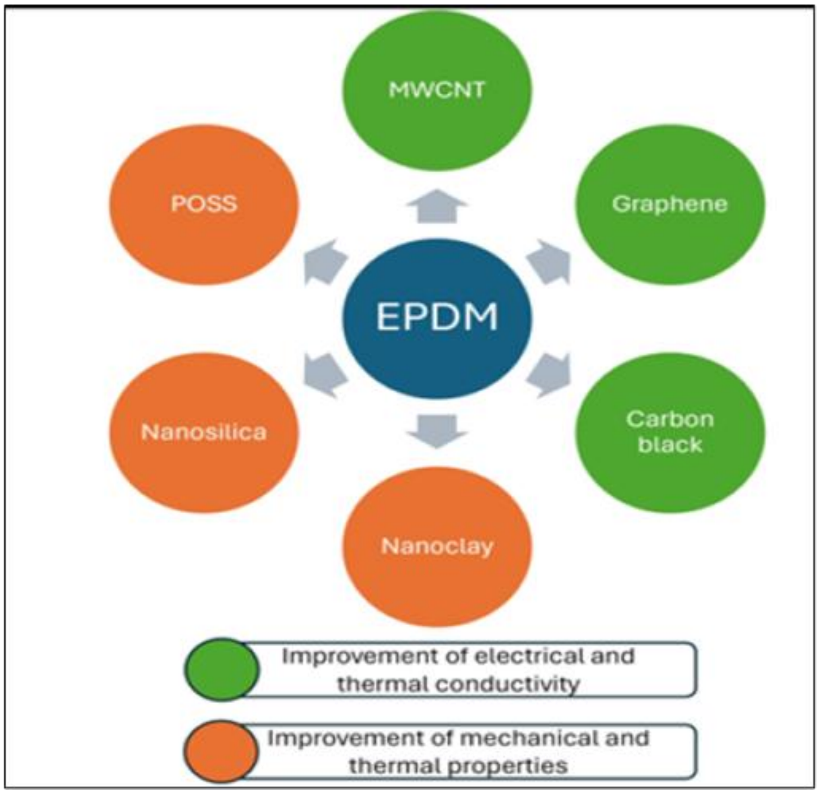

Figure 1: Flowchart of EPDM-Based Nanocomposite with Different Nanofillers and their Effect on its Properties.

Table 1: Features of Used Nanoparticles (Silica, Graphene, CNTs) in Diaphragms Manufactured by EPDM Rubber Composites Enhancement.

Property	Relevance to Diaphragms	Nanoparticle Role
Tensile & Tear Strength	Withstand repeated deflection	Graphene & CNTs improve load-bearing
Fatigue Life	Prevent cracking under cyclic flexing	CNTs delay crack initiation/spread
Gas Permeability	Prevent air/fluid leakage	Graphene reduces gas permeability
Thermal Resistance	High-temperature service	Silica & graphene enhance heat stability
Chemical Resistance	Fluids, oils, brake fluids, etc.	EPDM is strong; nanosilica helps even more
Modulus Tuning	Control flexibility vs stiffness	Ratio of carbon black vs nanofillers

3.1 Analytical Modeling

The analytical model is a semi-empirical formulation based on material mechanics and reinforcement theory. It is designed to predict the influence of nanofiller content on mechanical properties.

The predicted elastic modulus of the composite-reinforced EPDM, E_c, can be calculated using the mixture rule.

$$E_c = E_m(1-\varphi) + E_f\varphi \tag{1}$$

In this context, φ denotes the filler volume fraction, while E_m and E_f represent the elastic modulus of the matrix and filler phases, respectively.

The mechanical properties were modeled using a nonlinear scaling relationship that accounts for filler efficiency and saturation effects. The general form of the model is expressed as:

$$P = P_o(1 + k\alpha - \beta k^2) \quad (2)$$

where P is the predicted property, P_0 is the base material property, k is the normalised filler content, and α and β coefficients represent the reinforcement efficiency and interaction effects. In this study, the material is considered homogeneous and isotropic at the macroscopic scale. The dispersion of nanofillers is assumed to be uniform within the matrix. Interfacial bonding between the filler and the matrix is implicitly accounted for in the efficiency factors. Temperature and strain-rate effects are incorporated via simplified correction factors. Nonlinear effects are approximated using a second-order polynomial term.

$$\sigma = \sigma_o(1 + C\ Log\ \dot{\varepsilon}) \quad (3)$$

- According to Basquin's formula, fatigue behavior is characterized by a power-law relationship between stress amplitude and the number of cycles to failure.

$$N_f = A.\sigma^{-m} \quad (4)$$

3.2 Experimental Work

This experimental work aims to develop EPDM rubber composites reinforced with multi-nanoparticle systems, including nanosilica, graphene, and carbon nanotubes. The goal is to enhance mechanical, thermal, and electrical properties through strategic filler incorporation. Standardized tests such as tensile, compression, impact, bending, and fatigue were conducted. The results provide insights into structure–property relationships for multifunctional rubber applications.

The material specifications and suppliers are given in Table 1. The composites were made with different weight fractions of nanoparticles using the hand lay-up molding technique.

Table 2 (a): The Materials Used Physical Properties

Material	Specification	Trade Name	Supplier
ZnO	Grade: > 99.7% ZnO; PbO ≤ 0.02%; MnO ≤ 0.0001%; CuO ≤ 0.001%; Cd ≤ 0.01%; Loss on ignition ~0.15%	(often generic)	Aslan Kauçuk (Turkey) standard ZnO activator
Cyclohexyl-Thio-Phthalimide	Purity ≥97–98%; melting point ~90–94 °C; heating loss ≤0.3%; ash ≤0.1%	Santogard PVI, PVI, CTP	Shandong/ China
Carbon	Particle size (nm): 109 DBP: 90 (ml/100g) Surface area: 34 (m^2/g) Aggregate size:252 (nm)	N660	Malaysia
Nano Graphene	Size of particle =10-30 nm, surface area=30-60 m^2/gm, Assay=99%)	Gnp	USA
Silica	Purity (%) 99.5, Average particle size 14-36 (nm), Specific surface area ($m^2\ g^{-1}$) 580±20, Microstructure shape: spherical, Poisson's ratio 0.18, Young's modulus (GPa) 70.	SiO_2	USA
Carbon Nanotubes	Diameter ~1.6 ± 0.4 nm, Length ≥ 5 µm (aspect ratio > 3000), Purity ≥ 80 wt %, or ≥ 99 % in concentrates, Surface Area ≥ 1,200 m^2/g, Young's Modulus ~100–500 GPa,	CNTs	USA
Ethylene Propylene Diene Monomer	Density: ~0.85–1.15 g/cm^3 depending on formulation, Tensile strength: ~7–20 MPa (≈ 500–2500 psi), Elongation at break: ~100–700 % (up to ~900 % in specific grades), Hardness range: Shore A 30–90	EPDM	Zhonghong/ China
Paraffinic Oil	Mass density 0.88 g/cm^3 at 20 °C), Viscosity:(8 cP)	-	Iraq

Table 2 (b): The Materials Used Physical Properties

Material	Specification	Trade Name	Supplier
Rubber Antioxidant	-	TMQ	Malaysia
Sulfur	-	-	Iraq
Benzothiazyl Disulfide	Melt Point: 172 °C Moisture / Heat Loss, %: < 0.5 Ash, %: < 0.3 Specific Gravity: 1.5 Dispersibility: Good (powder & pellets)	MBTS	KSA

3.2.1 Compound Recipes

Tables 2 show the matrix of EPDM composites at different concentrations of three types of nanoparticles (0, 1, 3, 4, and 5 phr). Carbon black was reduced slightly as nanoparticle phr increased, to keep total filler ~40 phr. Nanoparticle composition (Xi) can be a 1:1:1 ratio of nanosilica: graphene nanoplatelets: multiwall carbon nanotubes (MWCNTs). Example: For 3 phr, use 1 phr of each nanoparticle.

Carbon black was reduced slightly as nanoparticle phr increased, to keep total filler ~40 phr. Antioxidant total was reduced from 4 to 2 phr (1 phr each of TMQ and 6PPD). Talc is a naturally occurring mineral composed mostly of hydrated magnesium silicate. It is widely used as an additive to polymers, to enhance mechanical properties, decrease cost and modify processing behavior. Talc fillers usually have superior stiffness and better dimensional stability, while the reinforcement is introduced to a lesser degree than in the case of nanofillers (CNT, graphene, silica).

Table 3: Recipes of EPDM Rubber Composites (Samples Loading Phr)

Ingredient	Sample No. 1	Sample No. 2	Sample No. 3	Sample No. 4	Sample No. 5
EPDM	100	100	100	100	100
Zinc Oxide (ZnO)	5	5	5	5	5
Stearic Acid	2	2	2	2	2
Antioxidant TMQ	1	1	1	1	1
Antioxidant 6PPD	1	1	1	1	1
Carbon Black	40	39	38	36.5	35
Nanoparticles (e.g.,1:1:1 Silica:Graphene: CNT)	0	1	2	3.5	5
Paraffinic Oil	20	20	20	20	20
MBTS (Accelerator)	2.5	2.5	2.5	2.5	2.5
Sulphur	2.5	2.5	2.5	2.5	2.5
CTP-100 (Scorch Retarder)	0.4	0.4	0.4	0.4	0.4

* x: (SiO_2, CNTs, Gnp)

3.2.2 Batches Design

Designing an EPDM rubber composite batch reinforced with three types of nanoparticles, such as nanosilica, graphene, and carbon nanotubes (CNTs), requires careful formulation to optimize dispersion, mechanical, and electrical properties without compromising flexibility or processability.

Below is a typical batch design example for lab-scale or pilot-scale formulation of EPDM composites reinforced with these nanofillers. This batch can be adjusted based on application goals (e.g., dielectric, EMI shielding, tensile reinforcement, or barrier properties).

3.2.3 Design Considerations for EPDM Nanocomposite Diaphragms

To fabricate diaphragm samples, a precision-designed mould was used to shape the EPDM nanocomposite into thin, flexible membranes with uniform thickness. The mould consists of upper and lower steel plates with a defined cavity and venting system to allow gas escape during curing. After vulcanization under controlled pressure and temperature, the diaphragms were demoulded and conditioned.

Figure 2 is a cross-section through a two-part mould assembly for producing elastomeric diaphragms, for example, by compression or transfer moulding. The molding device comprises two essential pieces: the upper half (Part No. 1022 01 000) and the lower half (Part No. 1022 02 000). The outer diameter of the mould is 305 mm.

The cavity formed between the two halves corresponds to the final shape of the diaphragm, which comprises several diameters, curved transitions, and inclined surfaces. The diaphragm has a cavity groove of Ø163 mm, Ø226 mm, and Ø255 mm. These dimensional increases likely correspond to different functional segments of the diaphragm.

The total thickness of the mould assembly is about 45 mm, with 32 mm of this thickness comprising the top portion, which is 5 mm below the top. There are R5 and R2.5 fillets inside for stress relief and easy demolding at key corners. These radii also permit the rubber to flow into the mold cavity more smoothly and evenly as it is compressed.

The cavity profile tapers, and the membrane is readily free from blockage after cure. These tools are used to help the rubber flow as the mold fills, thus minimizing any air entrainment or other defects.

Two line-up holes for Ø9.1 mm pins have been designed on the mould. 1: mm, placed on one pitch circle Ø 254.5 mm before stretched. They are used to maintain cavity concentricity and accuracy when closing the halves, provided that the upper and lower halves are correctly positioned relative to each other.

From this viewpoint, no distinct heating passages or discharging grooves are described; recognition is provided for external heating or other aspects from yet another view. But the mould appears to have tight machining tolerances and a nice parting line, which could act as vents during formation.

The mould is generally used to make diaphragms for control valves, actuators, pneumatic pumps, or other pressure-actuated equipment. The right transition and accurate cavity enable the diaphragm to meet the performance requirements of flex, pressure resistance, and sealing.

Tooling is centered around dimensional stability, material flow dynamics, and high-speed production, and is particularly suitable for medium to large volumes of Diaphragm production.

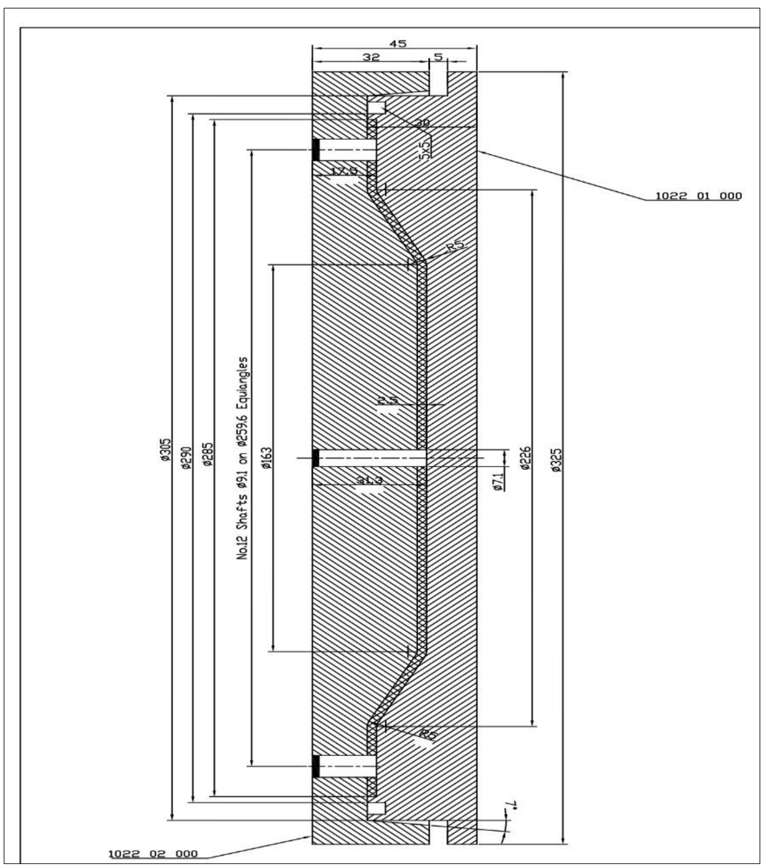

a.

b.

Figure 2. a. The Designed Mould for Producing an EPDM Rubber Diaphragm for the Hydraulic System, b. The Diaphragm Produced

In this work, EPDM N-diaphragms, typically thickened from 0.5 to 2 mm and with hardness Shore A 40 to 80, depending on stiffness requirements, are used. Compression set <20%, and modulus manipulation is required to modulate the CB/nanoparticle ratios to attain a good mechanical, stiffer/elastic balance, to maintain the dynamic deflection constant and prevent cracking. A custom pressurised chamber was then made to check mechanical performance under working conditions. Each diaphragm was clamped and forced to increase internal air or fluid pressure with a calibrated hydraulic or pneumatic system. The maximum pressure sustained before rupture was noted to determine burst strength and mode of failure against these simulated service conditions. The mould design used is depicted in Figure 2.

3.2.4 Sample Preparation

Rheological tests were conducted on the compound without curing the samples. The tests were performed inside the machine, which includes curing time, burning, viscosity, and torque. Samples were directly taken from the prepared compound, and a disc with a diameter of 40 mm and a thickness of 6 mm was prepared using a sample press machine, as shown in Figure 1.

Figure 3: The Typical Arrangement for 3 Rheological Tests.

The samples are placed in their designated position in the rheometer, under specific conditions: a curing time of 15 minutes, a pressure of 500 psi, and a temperature of 160°C. The test results are then obtained for the curing time (t90), scorch time (tS2), viscosity, and torque**.**

For the preparation method of physical property test samples (specific gravity and hardness tests), the sample is vulcanised in a testing mould designed explicitly for this purpose to ensure the accuracy and reliability of the results, and then pressed using a hydraulic press. The dimensions of the sample are 45 mm in diameter and 3 mm in thickness for the hardness and specific gravity tests, as shown in Figure 2.

3.2.5 Experimental Tests

The experimental work includes conducting various tests, such as:

- Compression using a uniaxial test with strain control**.**
- Three-point bending setup to monitor stress-strain behavior**.**
- Izod impact test to evaluate toughness**.**
- Cyclic loading to determine life cycles under constant amplitude stress.

3.2.5.1 A. Tensile Testing

Some of the properties determined are Strength, Stretchability, and Flexibility in the finalized product expressed by: Tensile strength at yield, Elongation at break, Modulus (100%, 200%, 300%) at 500 mm/min. A test piece according to ASTM D412 is generally dumbbell-shaped, with overall dimensions of 115 mm in length and a thin portion of (33 mm × 6 mm × 2 mm). For forming, a mould-cured rubber sheet (approximately 2 mm in thickness) is formed by hot pressing (160°C, 10–15 min). Furthermore, dumbbell specimens were cut using an ASTM die cutter. A universal testing machine (UTM) with a 500 N or 10 kN load cell and a crosshead speed = 500 mm/min was used to collect stress-strain curves to ensure the reliability and uniformity of the test process.

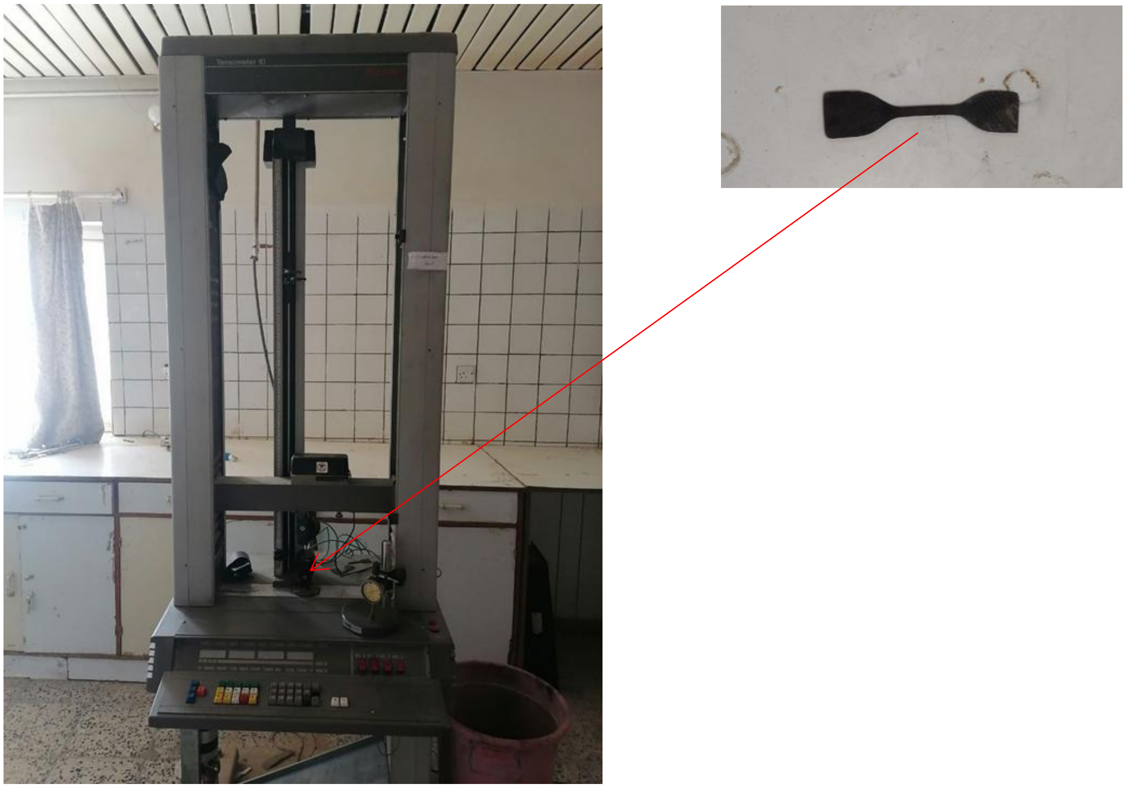

Figure 4: The Tensile Test Setup

3.2.5.2 B. Compression Testing

Includes measures of deformation resistance under compressive loads, used for gaskets, seals, and vibration-damping materials. Sample preparation is based on the standard ASTM D575. Specimen: cylindrical disc with dimensions ~29 mm diameter × 12.5 mm thick. Use a compression mold or punch cylindrical specimens from cured EPDM. Ensure flat, parallel surfaces. The UTM with compression plates is used to compress the sample to a fixed strain (e.g., 25%) and record the stress response. Alternatively, record load vs. displacement until failure.

3.2.5.3 C. Impact Testing

To measure a material's ability (e.g., boots, seals, bumpers) to absorb sudden energy and resist fracture under high-speed loading, an impact test is used. To prepare a sample, a standard ASTM D256 (Izod) notched beam with dimensions 63.5 mm × 12.7 mm × 3.2 mm (standard Izod) is used. A Mold and cut rectangular strips are used to produce notched specimens in the center using a notch cutter (notch depth ~2.54 mm). The Pendulum impact tester (Izod/Charpy) is used by mounting the specimen vertically (Izod) or horizontally (Charpy) and recording the energy absorbed (Joules) at fracture.

3.2.5.4 D. Flexural / Bending Testing

Assesses rigidity and flexural strength, especially important when evaluating stiffness after filler addition. Samples with rectangular beams have dimensions (127 × 12.7 × 3.2) mm and are fabricated according to ASTM D790 to conduct 3-point bending using a UTM. The span length is 100 mm, and the crosshead speed is 2 mm/min. This test allows for recording the maximum load and calculating flexural strength and modulus.

3.2.5.5 E. Fatigue Testing

The testing procedure is meticulous, evaluating the material's resistance to cyclic loading, which is necessary for dynamic sealing, tyres, and anti-vibration parts. It records crack creation and multiplication due to repeated stresses. Sample preparation is done according to the standard ASTM D4482 (for rubber fatigue), and a Dumbbell or rectangular strip (similar to tensile) is used as the specimen. The rubber fatigue machine, which functions at a precise frequency of 1–5 Hz, with a strain level of 20–50%, and is capable of cycles up to 10^5–10^6, will be used to perform this testing. One can obtain the number of cycles to failure and crack propagation rate (if using notched samples), which indicates once more the accuracy of the process.

Figure 5: The Fatigue Test Setup

3.3 Statistical Analysis

Using a statistical methodology, the models were tested for accuracy and reliability by comparing predicted outcomes with experimental data. A quantitative assessment of the performance of the respective models was done using the coefficient of determination (R^2) to measure correlation and root mean square error (RMSE) to quantify deviation. That experimental data is the reference (ground truth) data. All errors are regarded as being randomly distributed. The dataset is considered sufficiently representative of the material behavior. For R^2, a linear correlation is assumed. Measurement uncertainties are not explicitly modeled.

The root mean square error is calculated as follows:

$$\text{RMSE} = \sqrt{\frac{1}{n}\sum(Exp - Model)^2} \tag{5}$$

While the coefficient of determination is:

$$R^2 = 1 - \frac{\sum(Exp-Model)^2}{\sum(Exp-Exp(avg.))^2}\sqrt{\frac{1}{n}\sum(Exp - Model)^2} \tag{6}$$

3.4 Finite Element Modeling

A finite element method (FEM) framework was generated to simulate the mechanical performance of an EPDM-based diaphragm under pneumatic pressure. This model applies continuum mechanics and nonlinear material modeling to accurately represent the hyperelastic response characteristic of rubber-like materials.

Numerical finite element modeling was used to mimic the diaphragm's mechanical response to pressure loading. The FEM model was created by solving the governing equilibrium equations of continuum mechanics on a discretized domain. For the nonlinear response of EPDM, a hyperelastic constitutive model (Mooney–Rivlin) was used. The diaphragm is described as an axisymmetric structure. The material response is purely hyperelastic without any viscoelastic effects. The loading condition is quasi-static with uniform pressure distribution. We assume fixed edges with no displacement as boundary conditions. Geometric simplifications reduce computational complexity.

The following equation describes the equilibrium of the system under quasi-static conditions:

$$\nabla\sigma + b = 0 \tag{7}$$

Here, σ denotes the Cauchy stress tensor and b represents body forces, which are neglected in this analysis. The formulation assumes axisymmetric deformation and uniform internal pressure loading. The weak, or variational, form of the governing equation is given as follows:

$$\int_{\Omega} \delta\epsilon : \sigma \, d\Omega = \int_{\Omega} \delta u . b \, d\Omega + \int_{\Gamma} \delta u . t \, d\Gamma \tag{8}$$

This formulation facilitates numerical discretization across the problem domain Ω, where δε denotes the virtual strain, δu denotes the virtual displacement, and t denotes surface tractions. Additionally, Γ denotes the boundary of the computational domain on which external tractions or prescribed boundary conditions are imposed.

A Mooney–Rivlin hyperelastic model was adopted to characterize the nonlinear elastic behavior of EPDM. The strain energy density function is defined as follows:

$$W = C_1(I_1 - 3) + C_2(I_2 - 3) \tag{9}$$

Here, C_1 and C_2 denote material constants, while I_1 and I_2 represent the invariants of the deformation tensor. This model is appropriate for analyzing large deformations in elastomeric materials. The constitutive relation for computing stress from deformation is as follows:

$$\sigma = 2(C_1 + C_2/\lambda) + (\lambda - 1/\lambda^2) \tag{10}$$

Here, λ denotes the stretch ratio. This relationship facilitates precise prediction of the nonlinear stress response under applied loading. The diaphragm geometry was discretized into finite elements, and the corresponding element stiffness matrix was determined as follows:

$$K_e = \int_{\Omega_e} B^T D B \, d\Omega \tag{11}$$

In this context, B denotes the strain–displacement matrix, while D represents the material constitutive matrix derived from the hyperelastic formulation. The global system of equations is subsequently assembled as follows:

$$Ku = F \tag{12}$$

Where K is the global stiffness matrix, u is the nodal displacement vector, and F is the external force vector due to the applied pressure. Boundary conditions were determined by constraining the edges of the diaphragm and applying a uniform internal pressure to the active surface. Numerical solutions were utilized to calculate the displacement and the stress distribution of the system. Finite element method (FEM) predictions were confirmed through bending measurements. It was found in the results that the simulation results show that the model can accurately predict the mechanical behavior of the diaphragm. Minor discrepancies were attributed to material simplifications and assumptions built into the numerical model.

The FEM uses a simplified axisymmetric formulation with one-dimensional discretization. This strategy considers the primary mechanical response of the diaphragm to pressure, but does not fully explain complex 3D deformation effects or viscoelastic behavior. Nevertheless, the model provides sufficiently accurate predictions for comparison and validation, since it agrees very well with experimental results.

4. Results and Discussion

The EPDM nanocomposites reinforced with different nanofillers were tested experimentally, modelled analytically, and simulated using finite element analysis. Results show increasing mechanical properties due to increasing content of nanofiller over the materials studied. FEA (Finite Element Analysis) of bending behavior was performed with a hyperelastic Mooney–Rivlin model to model the deflection of diaphragm under pressure applied. The FEA prediction results are highly compatible with the experimental data, confirming that this numerical analysis method successfully models the nonlinear deformation response of EPDM-based diaphragms. Compression, impact, and fatigue data were calculated by analytical modeling for the entire range of nanofiller concentrations (0–5 wt%). The modeling reflected experimental trends as all the properties show progressive enhancement caused by the strengthening effect of the nanofillers. Graphene showed the highest improvement observed among the materials tested, followed by carbon nanotubes (CNT) and silica based on their reinforcement effectiveness. Error analysis demonstrated that the deviations between the experimental and the modeled values were acceptable regardless of the scenario investigated. Statistical evaluation based on the coefficient of determination (R^2) and root mean square error (RMSE) confirmed the high accuracy of the proposed model. It showed a strong correlation between predicted and experimental values. The correlation plots indicated that most values align closely with the ideal line of agreement, indicating that the model accurately captures the material response. Small variations in impact and fatigue response are ascribed to complicated failure mechanisms and microstructural contributions that are not fully explained in the simplified analytical formulation. The integration of experimental, analytical, and numerical findings provides a holistic image of EPDM nanocomposite mechanical properties. The proposed model enables realistic and efficient prediction of material performance, eliminating the need for very large-scale experimental testing.

Figure 6 reveals the non-linear stress-strain behaviour of EPDM base compounds containing 1 wt % of filler. The highest stresses are obtained for composite EPDM with graphene (the best reinforcement). The CNT-filled EPDM also performs well when compared to graphene, slightly below graphene, since it transfers loads well. In comparison to the other two EPDMs, the silica-filled EPDM shows the lowest stress response. None of the curves shows a linear material response, with the rubber-type nonlinearity of EPDM. For the same loading, Graphene > CNT > Silica with reinforcement efficacy. At the 50% strain the strength is for Graphene 1.62 MPa, for CNT 1.60 MPa, for Silica around the 1.57 MPa. is the optimal stress of graphene/EPDM, which has the highest reinforcement. CNT-EPDM didn’t do as well as the graphene (about 1.60 MPa at 50% strain).

For instance, under consistency with the same strain, silica-filled EPD M has the minimum stress ~1.57 MPa. All the composites display rubber-like nonlinear elasticity. In other words, Graphene > CNT > Silica in mechanical properties for 1 wt % loading.

The data presented in Figure 7 reveal a linear rise in tensile modulus with CNT weight%. At 0 wt%, modulus is 3.5 MPa, to 7.4 MPa at 5 wt%. This shows good reinforcement of EPDM by CNTs. This strong linear trend indicates an even dispersion and interaction. Increased CNT loading greatly improves the stiffness of the composite. Moreover Figure 8 illustrates linear behavior for tensile modulus with an increase in silica concentration. At 0 wt%, the modulus is 3.5 MPa and rises to 7 MP at 5 wt% silica. Silica is a very efficient reinforcing filler for EPDM, stiffness increases with continous raising of weight fraction. The linearity corresponds to a good dispersion and a matrix interaction. This increment is nonetheless slightly lower than that using CNT for the same loadings.

The tensile modulus can be easily extracted from the plot observed in Figure 9, where graphene content increases linearly. Modulus rises from ∼3.5 MPa at 0 wt% to ∼7.3 MPa at 5 wt% graphene. Graphene gives strong support because of its high aspect ratio and surface area. The linear nature also indicates the homogeneous distribution and excellent interfacial bonding. At any given loading, graphene provides a higher modulus than either filler.

The data presented in Figure 10 indicates a substantial difference of the mechanical performance, with the highest normalized value determined for Impact resistance (~ 12.2), and consequently for energy absorption capability. Both bending and compression strengths are moderate around of 4.4 and 3.6, respectively, revealing good rigidity and carrying ability in terms of static loading. Fatigue performance (normalised to a 10^5 scale) is significantly lower (~1.7), indicating possible susceptibility to cyclic loads. This difference could be attributed to details of microstructure, such as high-impact-toughness phases or crack-arrest features which do not promote fatigue resistance. The higher impact property indicates potential use in applications requiring high toughness such as protective casings or crashworthy structures. More fractographic and microstructural examination is suggested to explain this low fatigue life.

According to Fig. 11, impact resistance is also the most significant mechanical property (~ 11.3), which shows great capacity for energy dissipation under dynamic stresses. Both bending and compression strengths are one step higher than in Figure 10, with values of about 3.8 and 4.5, respectively, indicating that the structure becomes less flexible. The Fatigue response remains relatively limited at 1.8, which further raises concerns about the long-term behaviour of the material under oscillating stresses. Better static properties are likely results from the denser matrix compaction or the modification of the fiber-matrix interfacial. Although static properties have been improved, given the durability limitation of fatigue, the development of fatigue-resistant reinforcement approaches including hybrid stacking, or surface treatment, is necessary. This also shows the necessity of composite designs tailored to engineering applications, seeking a compromise between impact strength and fatigue resistance.

Also from Figure 12, it is seen that the mechanical behavior remains similar to those presented in the previous figures: the Impact strength dominates (~ 11.7), the bending (~ 4.2) and compression (~ 3.4) are moderate. The fatigue behavior (~ 1.8) does not greatly improve, indicating the weakness to fatigue is inherent to base material or architecture.” A consistent behaviour is seen between all 3 figures, which suggests the existence of an anisotropic structure or microcrack initiation at low stress cycles. The high impact strength implies a possible further use as a shock absorber, except possibly in fatigue-critical applications. These results suggest that the failure modes in cyclic loading are not the same as those in impact resistance and vice versa, meaning that, as is likely the case for the well-known dual-mode materials reinforcement system, both types of reinforcement are necessary. A multimodal testing and modelling strategy is necessary to predict service life under fatigue loading conditions.

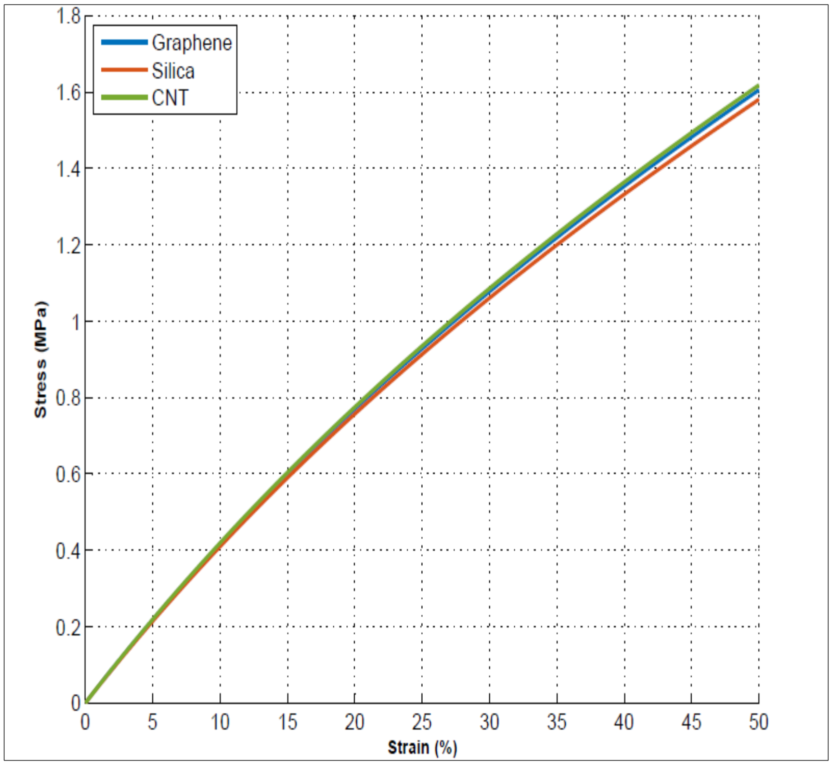

Figure 6: Nonlinear Stress-Strain Behavior at 1 wt% Nanoparticles

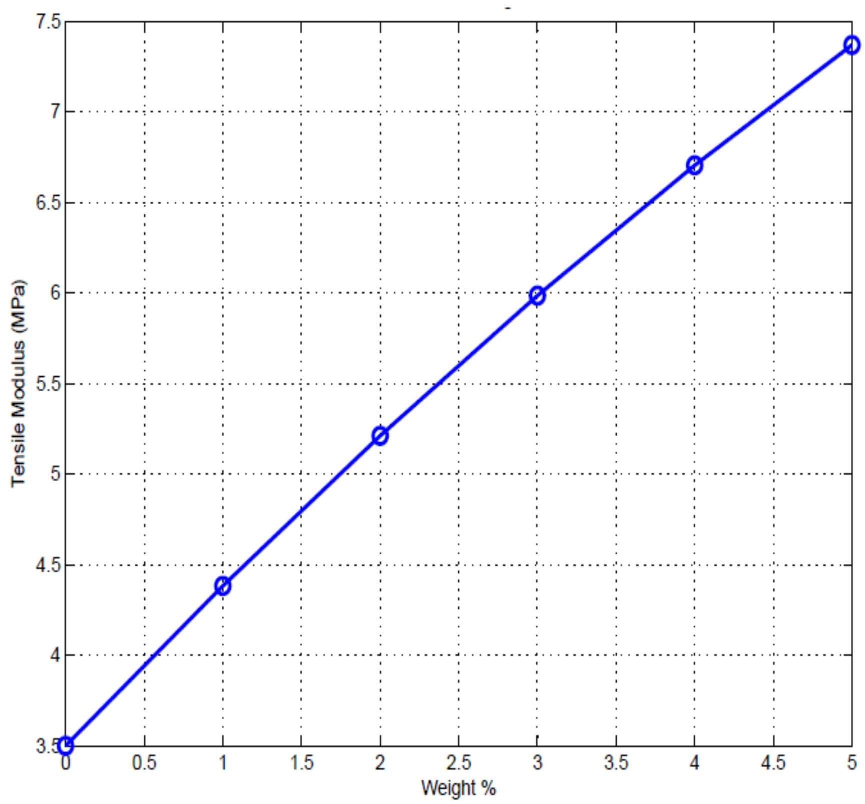

Figure 7: Tensile Modulus vs Weight % - CNT

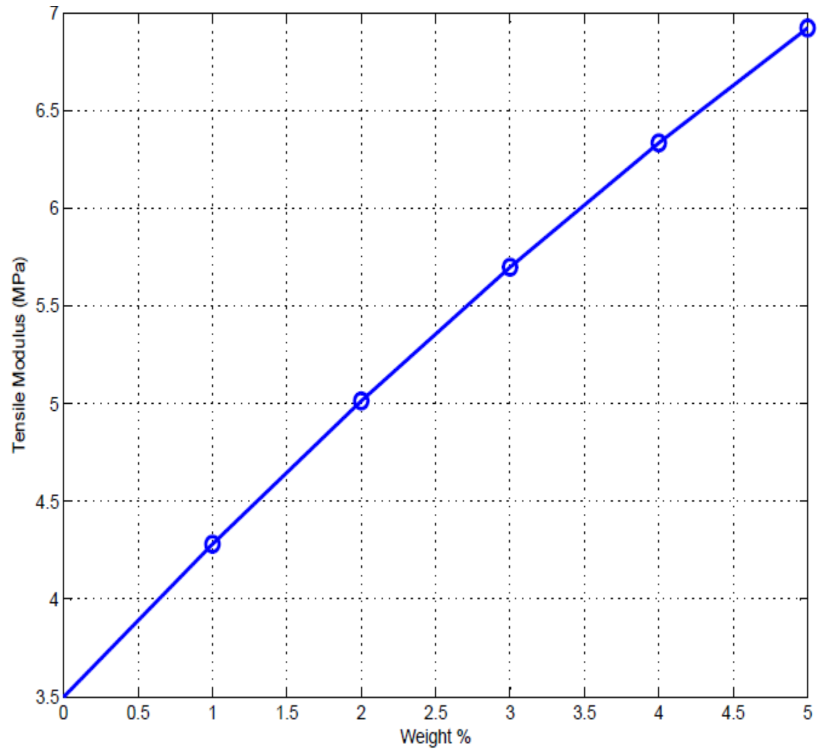

Figure 8: Tensile Modulus vs Weight % - Silica

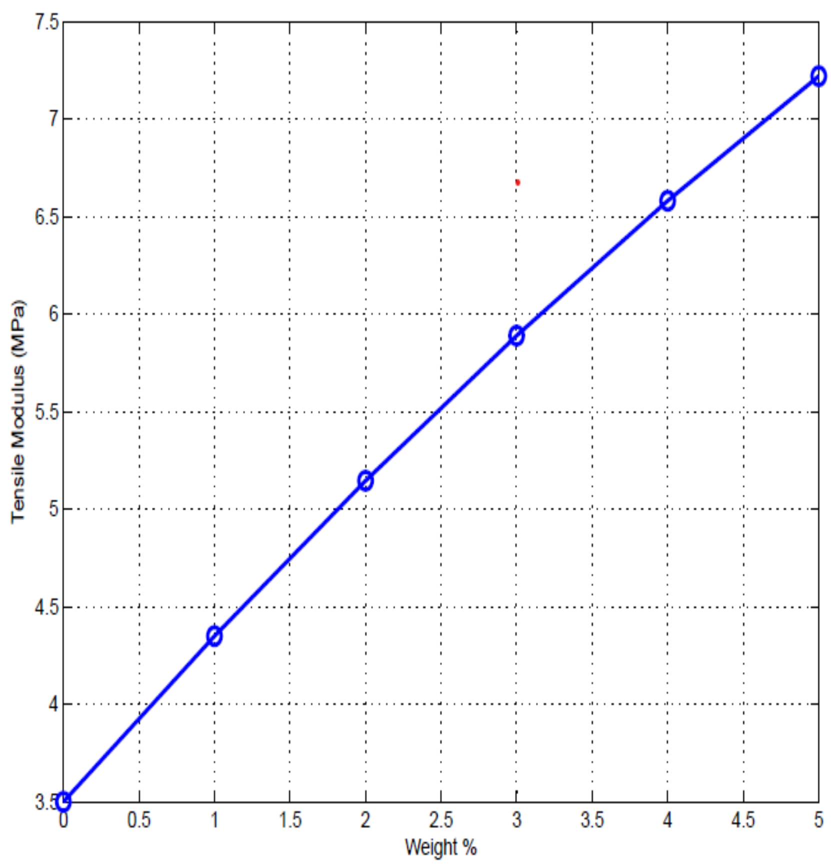

Figure 9: Tensile Modulus vs Weight % - Graphene

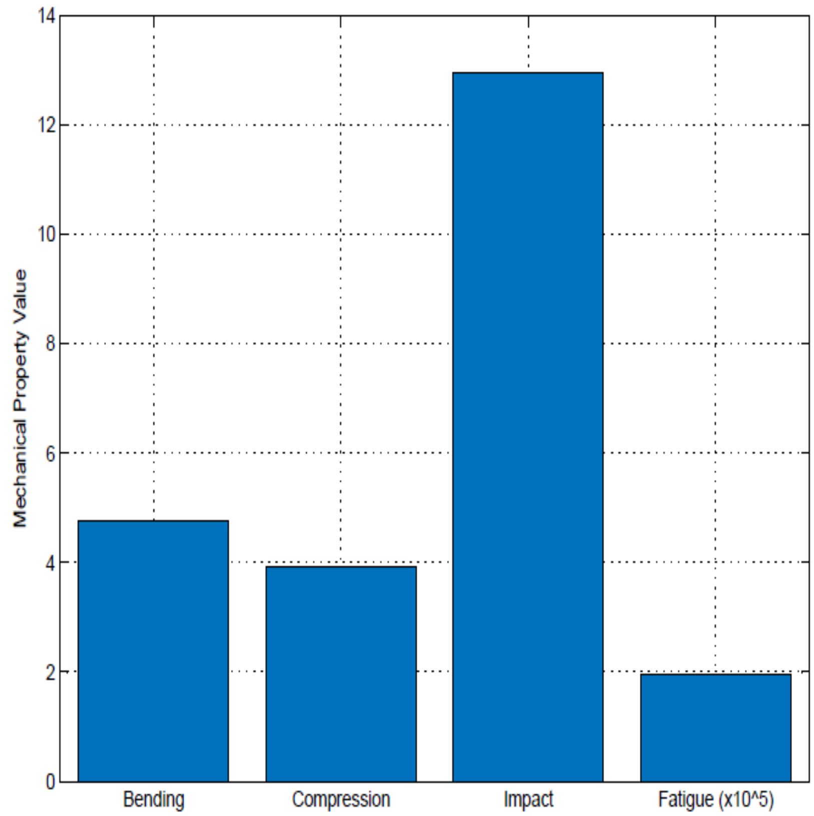

Figure 10: Estimated Mechanical Properties at 2 wt% of Graphene Nanoparticles, Strain Rate 0.03 (1/s)

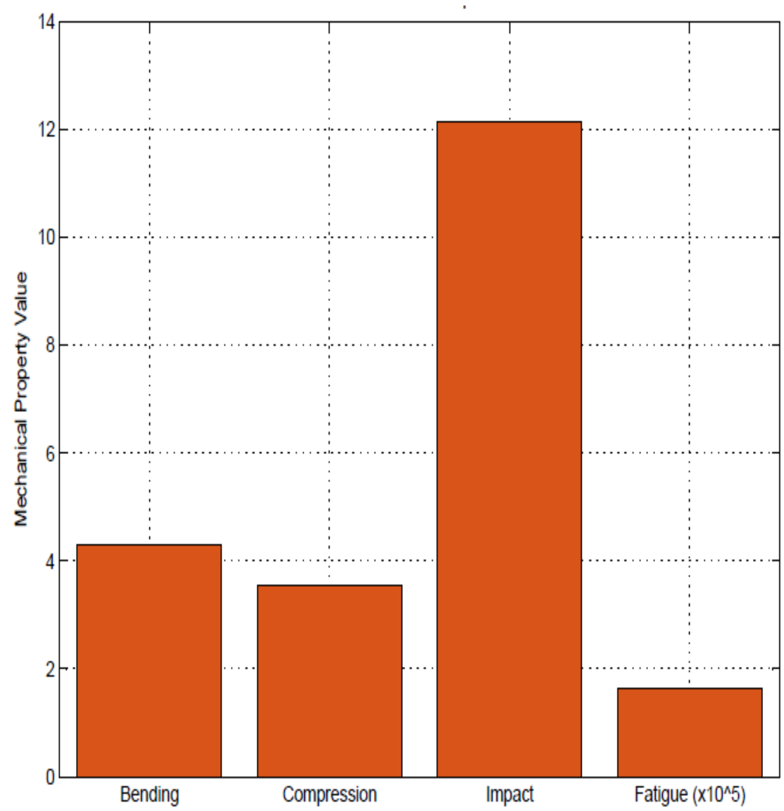

Figure 11: Estimated Mechanical Properties at 2 wt% of Silica Nanoparticles, Strain Rate 0.03 (1/s)

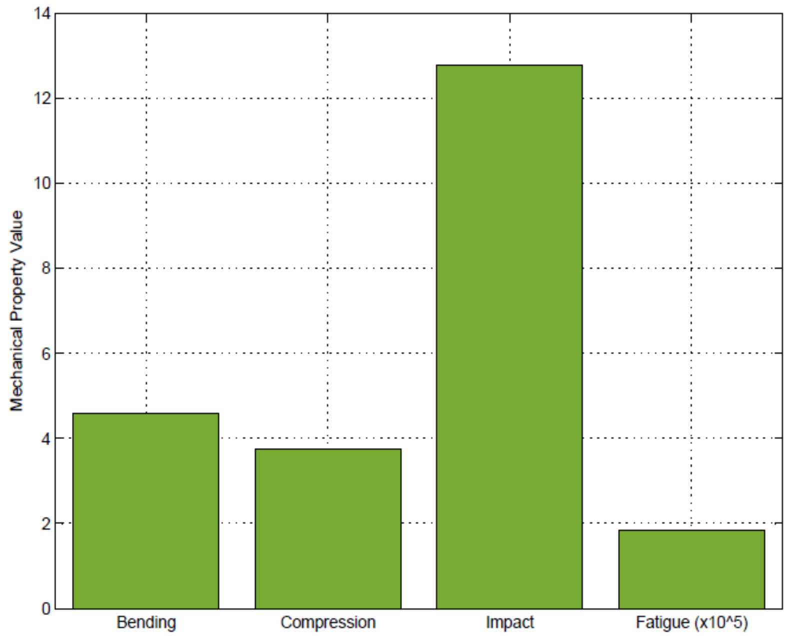

Figure 12: Estimated Mechanical Properties at 2 wt% of Carbon Nanotubes, Strain Rate 0.03 (1/s)

From Fig. 13, at 5 wt%, CNT possesses the optimal overall mechanical properties for the fillers. The properties are enhanced to an extent by graphene however graphene is a little behind CNT in all properties. The lowest flexible and compressive moduli, and the impact and fatigue equation parameters, are found with silica. Impact is one of the fillers with the highest impact strength, CNT has ~20.2 units. The more effective reinforcement by CNT is possibly attributed to its higher aspect ratio and load transfer efficiency. However, according to Fig. 14, the mechanical properties of 5 wt% graphene, Silica, CNT, and Carbon Black are compared. CNT has the highest fatigue and impact performance, just followed by Graphene. Carbon Black presents the lower values for the all features, and the most significant ones are fatigue. Silica shows average performance, but it is behind CNT and Graphene overall. Overall, the mechanical reinforcement is much more efficient by using nanofillers (e.g., Graphene, CNT, Silica) than CBN. The mechanical chart shown in Fig. 15 illustrates a comparison between Graphene, Silica, CNT, and Talc at 5 wt%. CNT has the highest impact and good fatigue properties, followed by Graphene. Talc has higher impact than Silica but inferior fatigue than both. For the range of properties considered, silica has values of the properties between CNT and Graphene and a modest set. CNT and Graphene demonstrate better reinforcement behaviour than Talc and Silica in general.

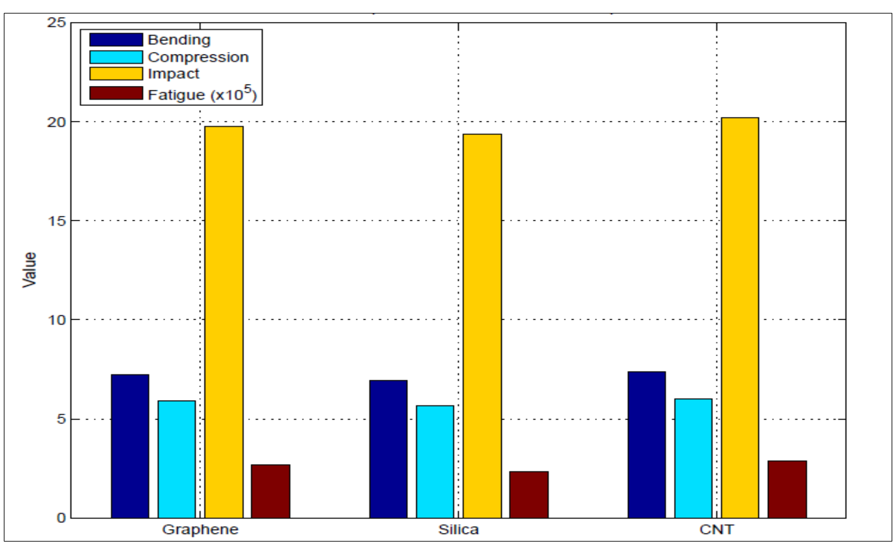

Figure 13: Mechanical Properties at 5 wt% for Each Nanparticles, Strain Rate 0.01 (1/s)

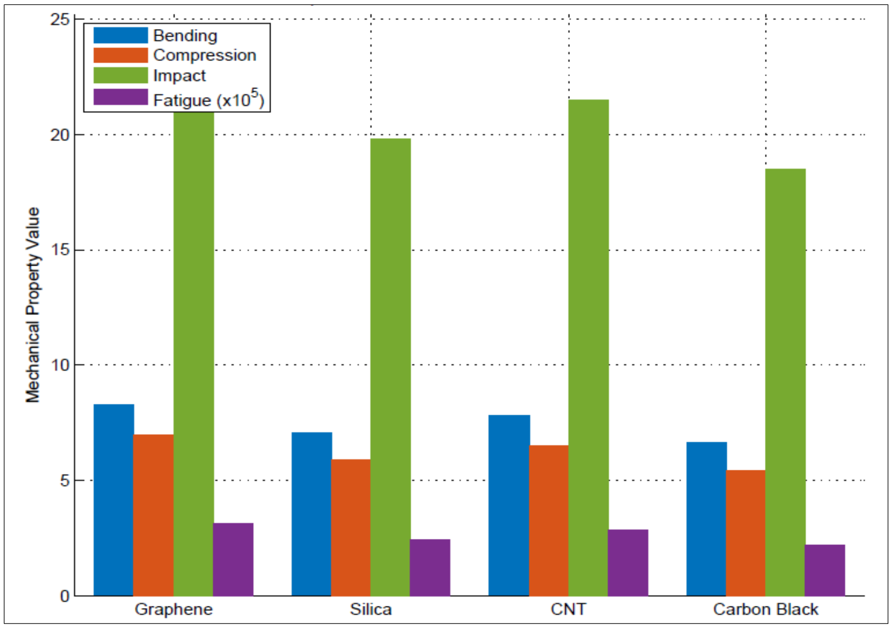

Figure 14: Comparison Nanofillers vs Carbon Black at 5 wt%

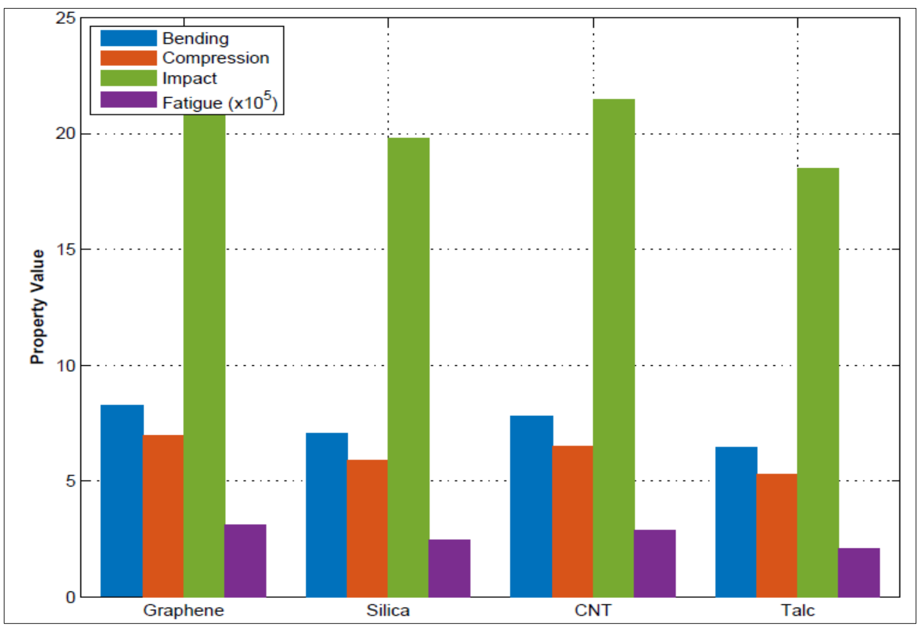

Figure 15: Comparison Nanofillers vs Talk at 5 wt%

From the results in Table 4, all nanofillers improve the properties of EPDM compared to neat EPDM. Bending (↑106%), compression (↑109%), impact (↑96%) and fatigue life (↑188%) are magnified by graphene. About CNTs, the performance of which is highest: the bending (↑111%), compression (↑115%), and impact (↑102%) strength is maximized and the fatigue life is enhanced to up to three times. Silica also improves performance to some extent, particularly fatigue life (↑114%) and impact resistance (↑77%), but not as much as CNT/Graphene. Talc provides a minimum reinforcement level of bending (↑85%), compression (↑89%), impact (↑85%), and fatigue (↑110%). Overall, CNT and Graphene are the best nanofillers, followed by Silica and Talc, for the least but useful results. Graphene and CNTs have strong interfibrillar bonding with EPDM, which provide the reinforcement effect. Because of their high aspect ratio and high mechanical resistance, CNT has slightly higher stiffness when compared to Graphene. However, graphene enhances the fatigue resistance, possibly owing to its layered structure and crack-bridging. Furthermore, the performance of silica is again observed to exhibit more uniform and moderate enhancements owing to the lower aspect ratio and good uniformity of dispersion. Here talc is only a filler, providing limited improvements, but not as good as potential of nanocarbon fillers.

Table 4: EPDM Nanocomposite Results

NPs	Wt%	Bending Modulus (MPa)	Compression Modulus (MPa)	Impact Strength (kJ/m^2)	Fatigue Life (cycles)
Graphene	0	3.5	2.8	10	100000
Graphene	1	4.34875	3.50616	12.231	138800
Graphene	2	5.145	4.16864	14.324	175200
Graphene	3	5.88875	4.78744	16.279	209200
Graphene	4	6.58	5.36256	18.096	240800
Graphene	5	7.21875	5.894	19.775	270000
Silica	0	3.5	2.8	10	100000
Silica	1	4.28085	3.45184	12.134	131040
Silica	2	5.0134	4.06336	14.136	160160
Silica	3	5.69765	4.63456	16.006	187360
Silica	4	6.3336	5.16544	17.744	212640
Silica	5	6.92125	5.656	19.35	236000
CNT	0	3.5	2.8	10	100000
CNT	1	4.3827	3.53332	12.328	142680
CNT	2	5.2108	4.22128	14.512	182720
CNT	3	5.9843	4.86388	16.552	220120
CNT	4	6.7032	5.46112	18.448	254880
CNT	5	7.3675	6.013	20.2	287000
Talc	0	3.5	2.8	10	100000
Talc	1	4.179	3.37036	11.94	125220
Talc	2	4.816	3.90544	13.76	148880
Talc	3	5.411	4.40524	15.46	170980
Talc	4	5.964	4.86976	17.04	191520
Talc	5	6.475	5.299	18.5	210500

Figure 16 compares measured mechanical properties from experiments with simulated mechanical properties obtained using the finite element method (FEM) for three nanocomposites at 5 wt%. Incorporating nanofillers significantly improves all measured mechanical properties. Carbon nanotubes (CNTs) exhibit the highest performance, followed by graphene, while silica offers moderate performance improvements. These trends are consistent across compression, impact resistance, and fatigue life, confirming that nanofiller reinforcement enhances the durability and structural reliability of EPDM composites. The superior performance of CNTs is likely due to their high aspect ratio and effective load-transfer capability.

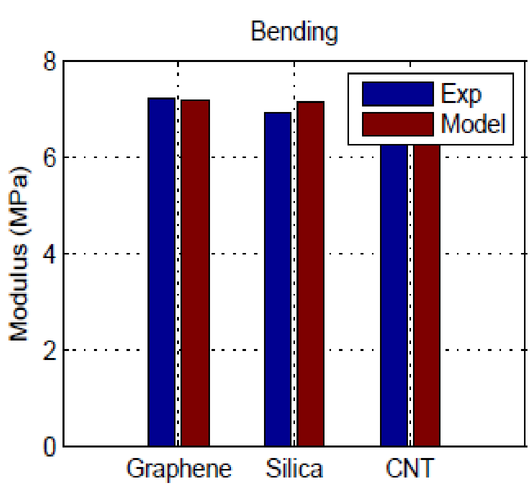

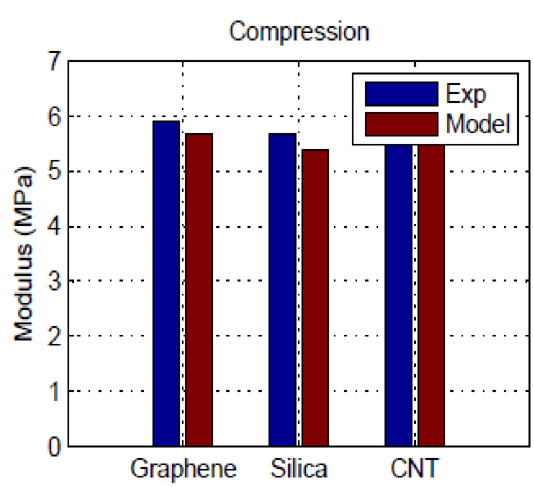

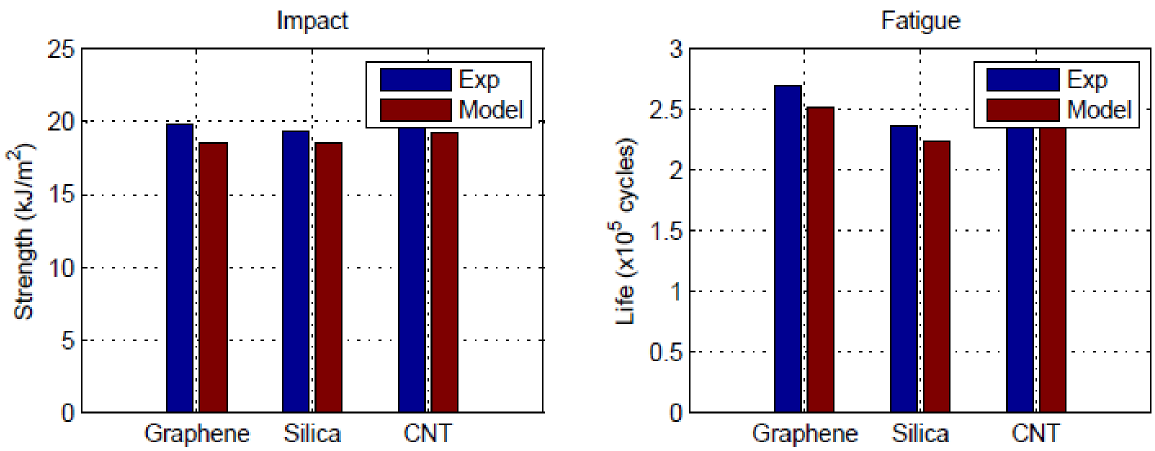

Figure 16: Comparison of FEM vs Experimental for (Bending, Compression, Impact, and Fatigue Life) using Different Nanofillers

Several statistical metrics were calculated, including the coefficient of determination (R^2) and root mean square error (RMSE), to assess the predictive performance of the proposed model. Table 5 shows a high correlation between experimental and predicted values, with an R2 value close to unity and a very low RMSE, confirming the reliability and accuracy of the model.

The statistical evaluation of the proposed model demonstrates strong predictive capability across all investigated mechanical properties. Among the investigated properties, bending and compression exhibit the highest accuracy. In contrast, slightly higher deviations observed in impact and fatigue behavior can be attributed to the complex and nonlinear nature of these properties, which are influenced by microstructural factors not fully captured in the simplified analytical model.

Figure 17 demonstrates the correlation between experimental and model results for flexibility, compression, impact, and fatigue life for all nanocomposites at 5wt%. The coloured correlation plots show that experimental and predicted results agree well for all nanofillers studied. There is significant convergence between graphene and CNT data points, indicating superior model consistency and reinforcement efficiency, whereas silica shows a higher but acceptable deviation. The results demonstrate that the proposed model accurately predicts the mechanical behavior of EPDM nanocomposites under a wide range of loading.

Table 5: Statistical Results of Mechanical Properties at 5 % wt.

Property	RMSE	R^2
Bending	0.412	0.893
Compression	0.432	0.83
Impact	0.908	0.927
Fatigue	0.156	0.927

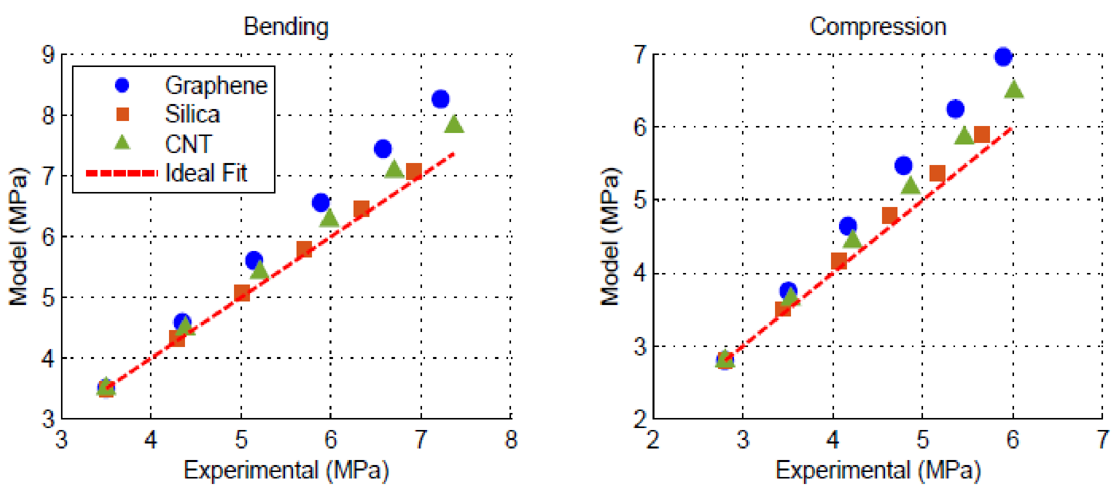

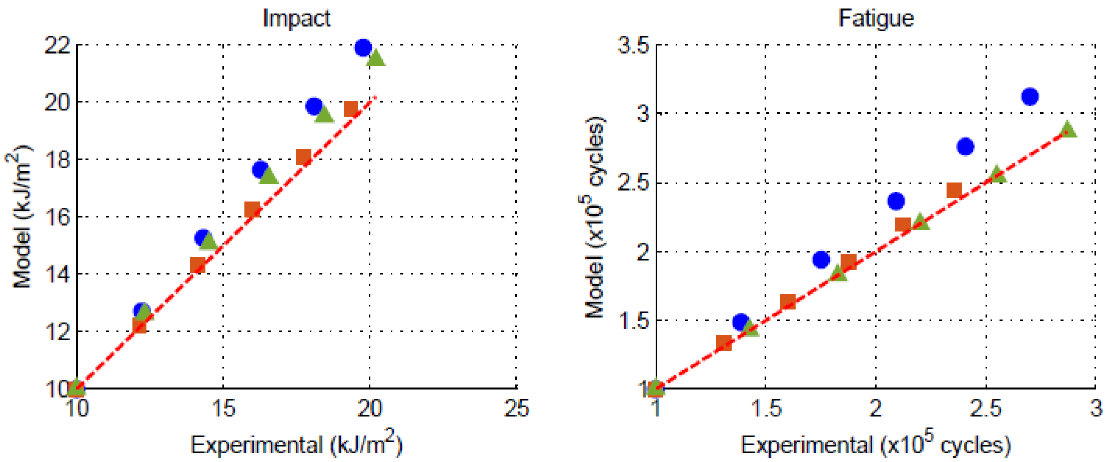

Figure 17: Correlation Between Experimental and Model Results for (Bending, Compression, Impact, and Fatigue Life) for the Full Set of Nanocomposites

5. Conclusions

The predicted results from both analytical and FEM models were validated against experimental data. Error analysis demonstrated that deviations remained within acceptable limits across all investigated cases. Furthermore, statistical evaluation using the coefficient of determination (R^2) and root mean square error (RMSE) confirmed a strong correlation between experimental and predicted results, indicating high model accuracy and reliability.

The results reveal that graphene exhibits the most significant enhancement in mechanical performance, followed by CNT and silica, highlighting the effectiveness of nanofiller reinforcement in EPDM matrices. The proposed integrated framework, combining experimental testing, analytical modeling, and FEM simulation, provides a robust and efficient tool for predicting material behavior and optimizing diaphragm design for industrial applications.

Preliminary results are expected to show enhanced mechanical performance of EPDM with increasing nanoparticle content up to an optimum level. However, agglomeration may reduce performance beyond a threshold. Based on the research results, the following conclusions can be made:

Nanofillers (Graphene, CNT, Silica) impart the mechanical properties for EPDM much higher than the conventional ones as Talc, Carbon Black.

CNT and Graphene are the nanofillers that generally exhibit the best reinforcement performance among others (tensile modulus, impact strength, flexural, compression, and fatigue resistance).

Generally, properties of the other substrates are improved but not usually as good as CNT and Graphene. All the nanofillers provide a linear rise in tensile modulus with filler loading, indicating good dispersion and stronger filler–matrix interaction.

CNT is the highest in terms of impact resistance and fatigue life; it is the most applicable for dynamic load applications.

The reinforcing results reported for Talc/CB are the poorest in the series (proved to be superior reinforcement in advanced composites). Unlike traditional fillers, the mechanical properties are barely enhanced with nanofillers (Graphene, CNT, Silica) only by a couple of. (For pressure swing adsorption in a shell-and-tube carbon fibre adsorbent-coated heat exchanger). In the EPDM industry, carbon black is preferred over talc for diaphragms due to its moderate surface area and superior reinforcement efficiency.

Nonlinear stress-strain analysis was also consistent with enhanced elasticity and strain-hardening for the nanofiller composites. The mechanical performance of CNTs/EPDM is the optimal, thereby also being an excellent reinforcement material in high-performance flexible structures. Talc and carbon black have low reinforcing capabilities, and nanofillers are preferable fillers for polymer composites.

Error analysis was conducted for all nanofiller concentrations, demonstrating that the proposed analytical model maintains consistent accuracy across the full range of compositions. In addition, the root mean square error (RMSE) values are relatively low for all properties, reflecting minimal deviation between predicted and experimental results. The deviations remain within acceptable limits, confirming the model's reliability.

Future work will include dynamic fatigue testing, thermal cycling, and life-cycle analysis for real-time industrial applications. Limitations include challenges with uniform dispersion and long-term environmental ageing effects.

References

Akrami, H., & Park, C. B. (2024). Advanced polycarbonate foam: Enhancing foamability and mechanical properties with toughened polycarbonate using nanofibrillation method and crosslinked rubbery EPDM networks. *Journal of Manufacturing Processes*, *127*, 340-348. https://doi.org/10.1016/j.jmapro.2024.07.105

Amani, A. M., Tayebi, L., Rezaeeparto, K., Parham, S., Azizli, M. J., Vafa, E., Kamyab, H., Rajendran, S., & Simancas-Racines, D. (2025). Enhancement of mechanical properties in ethylene propylene diene monomer/natural rubber nanocomposites through Ti3C2TX reinforcement and EPDM-g-MAH compatibilization. *Diamond and Related Materials*, *157*, 112535. https://doi.org/10.1016/j.diamond.2025.112535

Azizli, M. J., Barghamadi, M., Rezaeeparto, K., Mokhtary, M., & Parham, S. (2020). Compatibility, mechanical and rheological properties of hybrid rubber NR/EPDM-g-MA/EPDM/graphene oxide nanocomposites: theoretical and experimental analyses. *Composites Communications*, *22*, 100442. https://doi.org/10.1016/j.coco.2020.100442

Bingöl, M. C., Yetgin, S. H., Köprü, İ., & Ulusal, F. (2025). Investigation of the properties of mesoporous-SiO2 filled EPDM (ethylene propylene diene monomer) rubber. *Inorganic Chemistry Communications*, *174*, 114061. https://doi.org/10.1016/j.inoche.2025.114061

Burgoa, A., Arrillaga, A., & Schreier-Alt, T. (2024). Effect of multiple recycling on thermo-mechanical and rheological behaviour of PP/EPDM thermoplastic vulcanizates. *Journal of Polymers and the Environment*, *32*(2), 947-961. https://doi.org/10.1007/s10924-023-03042-2

Colom, X., Marín, M., Saeb, M. R., Formela, K., & Cañavate, J. (2024). Recycling devulcanized EPDM to improve engineering properties of SBR rubber compounds. *Resources, Conservation & Recycling Advances*, *23*, 200227. https://doi.org/10.1016/j.rcradv.2024.200227

Cui, Z., Liu, W., Tan, L., Sun, G., & Hu, X. (2024). Evidence for non-Arrhenius behavior of EPDM rubber by combining Arrhenius and time–temperature superposition (TTS) extrapolations. *RSC advances*, *14*(8), 5216-5221. https://doi.org/10.1039/d3ra07159f

de Souza, E. L., de Sousa Zanzi, M., de Paiva, K. V., Oliveira, J. L. G., de Oliveira Barra, G. M., & Dutra, G. B. (2025). Experimental and numerical analyses of thermo-oxidative aging in NBR and EPDM rubber with different lengths. *Polymer*, *334*, 128694. https://doi.org/10.1016/j.polymer.2025.128694

Du, X., Li, F., Qin, F., Chu, J., Dang, W., Hu, X., Zhang, X., Zhao, K., & Tang, Y. (2025). A review of ceramizable EPDM composites: Current status and future perspectives. *Polymer Degradation and Stability*, *238*, 111345. https://doi.org/10.1016/j.polymdegradstab.2025.111345

Eyssa, H., Maziad, N. A., Kansouh, W., & Ramadan, W. (2024). Neutron attenuation performance of EPDM rubber with BN Nanoparticles/B2O3 composite and studying physical, thermal and mechanical properties. *Nuclear Engineering and Technology*, *56*(11), 4563-4577. https://doi.org/10.1016/j.net.2024.06.019

Fang, W., Cai, Y., Zhu, J., Ma, Y., Gou, H., Wang, H., & Fan, H. (2025). Preparation of polysiloxane-functionalized polyolefin with unsaturated groups for improving the compatibility of EPDM/silicone rubber blends. *European Polymer Journal*, *234*, 114029. https://doi.org/10.1016/j.eurpolymj.2025.114029

Foltuț, D., Uțu, I.-D., & Șerban, V.-A. (2025). Tribological Performance of EPDM and TPV Elastomers Against Glass Fiber-Reinforced Polyamide 66 Composites. *Materials*, *18*(11), 2515. https://doi.org/10.3390/ma18112515

Gong, C., Xie, C., Zhu, H., Ding, W., Song, J., & Ge, Y. (2024). Time-varying compressive properties and constitutive model of EPDM rubber materials for tunnel gasketed joint. *Construction and Building Materials*, *433*, 136734. https://doi.org/10.1016/j.conbuildmat.2024.136734

Gupta, P., Chattopadhyay, S., & Das, N. C. (2025). Short fiber reinforced elastomeric composites with enhanced mechanical and tribological properties for potential application in V-belts. *Frontiers in Mechanical Engineering*, *11*, 1629780. https://doi.org/10.3389/fmech.2025.1629780

Hayeemasae, N., & Ismail, H. (2023). Comparative Studies of Natural Rubber/Virgin Ethylene Propylene Diene Rubber and Natural Rubber/Recycled Ethylene Propylene Diene Rubber and Natural Rubber/Blends. In *Recycled Polymer Blends and Composites: Processing, Properties, and Applications* (pp. 179-207). Springer. https://doi.org/10.1007/978-3-031-37046-5_9

Hou, N., Guo, Q., Zairi, F., Tian, L., & Ding, N. (2025). Predicting viscoelastic behavior and crack propagation in EPDM rubber under long-term thermal aging. *Engineering Fracture Mechanics*, *315*, 110782. https://doi.org/10.1016/j.engfracmech.2024.110782

Khaleel, H. H., & Al-Hadrayi, Z. M. (2025). Free Vibration Analysis of Rotating Functionally Graded Material Beams on Elastic Foundations Using the Homotopy Perturbation Method. *Mathematical Modelling of Engineering Problems*, *12*(8). https://doi.org/10.18280/mmep.120818

Khozemy, E. E., Nasef, S. M., & Radi, H. (2024). A comparative study of the mechanical and thermal properties of EPDM rubber/cement kiln dust composite cured by ionizing radiation. *International Journal of Polymer Analysis and Characterization*, *29*(5), 282-299. https://doi.org/10.1080/1023666X.2024.2360855

Kiran, L. P., Venkataramiah, P., & Rani, S. U. (2023). Experimental study of vibration attenuation at rail joints by using Ethylene propylene Diene Monomer (EPDM) rubber. *Materials Today: Proceedings*, *80*, 1317-1326. https://doi.org/10.1016/j.matpr.2023.01.063

Lee, S.-H., Yang, S.-W., Park, E.-S., Hwang, J.-Y., & Lee, D.-S. (2019). High-performance adhesives based on maleic anhydride-g-EPDM rubbers and polybutene for laminating cast polypropylene film and aluminum foil. *Coatings*, *9*(1), 61. https://doi.org/10.3390/coatings9010061

Li, X., & Gong, Z. (2024). Investigation of long-term waterproof performance and hardness change of EPDM rubber gasket used for shield tunnels. *Journal of Materials in Civil Engineering*, *36*(2), 04023577. https://doi.org/10.1061/JMCEE7.MTENG-16744

Ling, Y., Liu, J., Xiao, B., Jin, H., Zhao, L., Bai, Y., Zhang, X., Liang, M., Chen, Y., & Zou, H. (2025). High mechanical interlocking and hydrogen bonding based carboxymethyl cellulose/SiO2 composite structures for interfacial bonding of reinforced polyimide fiber/EPDM composites. *Composites Part B: Engineering*, *304*, 112652. https://doi.org/10.1016/j.compositesb.2025.112652

Luo, Y., Wang, X., Ding, J., & Chen, Y. (2025). Large-scale recycling of waste cross-linked ethylene propylene diene monomer enabled by devulcanization-grafting strategy. *Polymer Engineering & Science*, *65*(6), 3163-3177. https://doi.org/10.1002/pen.27206

Marin-Genesca, M., Garcia-Amoros, J., Mudarra, M., Massagués Vidal, L., Canavate, J., & Colom, X. (2023). Insights into the structural and dielectric behavior of composites produced from EPDM waste processed through a devulcanization method and SBR. *ACS omega*, *8*(14), 12830-12841. https://doi.org/10.1021/acsomega.2c08115

Moustafa, H., Lawandy, S. N., Rabee, M., & Zahran, M. A. (2020). Effect of green modification of nanoclay on the adhesion behavior of EPDM rubber to polyester fabric. *International Journal of Adhesion and Adhesives*, *100*, 102617. https://doi.org/10.1016/j.ijadhadh.2020.102617

Mukhopadhyay, A., & Roy, D. (2023). Study on abrasive wear pattern of ethylene propylene dyne monomer (EPDM) rubber compound. *Materials Today: Proceedings*, *78*, 476-480. https://doi.org/10.1016/j.matpr.2022.10.297

Ndour, I., Mougne, Q., Falzon, M. F., & Richaud, E. (2025). Thermal ageing of PP-EPDM thermoplastic vulcanizate: Multiscale study and kinetic modeling. *Polymer Degradation and Stability*, *240*, 111478. https://doi.org/10.1016/j.polymdegradstab.2025.111478

Prut, E. V., Solomatin, D. V., & Kuznetsova, O. P. (2017). Rheological behaviors of blends based on polypropylene and EPDM rubber powder. *Mendeleev Communications*, *27*(3), 318-320. https://doi.org/10.1016/j.mencom.2017.05.035

Sharma, S. K., Miladinović, S., Sharma, L. K., Gajević, S., Sharma, Y., Sharma, M., Čukić, S., & Stojanović, B. (2026). Graphene/CNT Nanocomposites: Processing, Properties, and Applications. *Nanomaterials*, *16*(2), 100. https://doi.org/10.3390/nano16020100

Simet, C., Mougin, K., Moreau, M., Perche, M., Vaulot, C., Ponche, A., & Bally–Le Gall, F. (2023). Investigation of ethylene-propylene-diene monomer (EPDM) ageing behaviour in PMDIs environment by surface NMR. *Polymer Testing*, *127*, 108171. https://doi.org/10.1016/j.polymertesting.2023.108171

Spanheimer, V., Šimić, D., Katrakova-Krüger, D., & Giese, U. (2025). Thermo-Oxidative Aging and Performance Comparison of Recovered, Sustainable, and Virgin Carbon Black in Ethylene Propylene Diene Monomer-Based Elastomers. *Macromolecular Materials and Engineering*, *310*(8), 2500034. https://doi.org/10.1002/mame.202500034

Spencer, M. P., Zwoster, A., Bisel, T. T., Murphy, M. K., & Fifield, L. S. (2020). Sequential versus Simultaneous Aging of EPDM Nuclear Cable Insulation Subjected to Elevated Temperature and Gamma Radiation. In *2020 IEEE Conference on Electrical Insulation and Dielectric Phenomena (CEIDP)* (pp. 470-474). IEEE. https://doi.org/10.1109/CEIDP49254.2020.9437502

Sumbodo, W., Pambudi, R., & Setiadi, R. (2025). Design and Analysis of Pick and Place Robot Gripper in the Fertilizer Industry. *Reports in Mechanical Engineering*, *6*(2), 53-64. https://doi.org/10.31181/rme511

Triganza, T., Refalo, P., Rochman, A., & Brancaleone, R. P. (2025). Process Parameter Optimization for Sustainable Manufacturing of Elastomeric Components Used in Water Treatment Systems. *Procedia CIRP*, *135*, 991-996. https://doi.org/10.1016/j.procir.2025.01.092

Vishvanathperumal, S., & Anand, G. (2021). Effect of nanosilica and crosslinking system on the mechanical properties and swelling resistance of EPDM/SBR nanocomposites with and without TESPT. *Silicon*, *13*(10), 3473-3497. https://doi.org/10.1007/s12633-020-00792-9

Wang, Q., Yao, M., Quan, Y., & Zhuang, D. (2024). Simultaneously achieving excellent heat aging resistance and grip performance in carbon black/glass flake/EPDM rubber composite for overhead line spacers. *Materials Today Communications*, *39*, 108878. https://doi.org/10.1016/j.mtcomm.2024.108878

Wang, Y., Li, J., Wan, L., Wang, L., & Li, K. (2023). A lightweight rubber foaming insulation reinforced by carbon nanotubes and carbon fibers for solid rocket motors. *Acta Astronautica*, *208*, 270-280. https://doi.org/10.1016/j.actaastro.2023.04.019

Wang, Z., Wang, J., Wu, H.-N., Zhang, R., Zhang, G.-y., Zhang, F., & Mariani, S. (2025). Investigation of the microstructure, mechanical properties and thermal degradation kinetics of EPDM under thermo-stress conditions used for joint sealing of floating prefabricated concrete platform of offshore wind power. *Construction and Building Materials*, *485*, 141897. https://doi.org/10.1016/j.conbuildmat.2025.141897

Xu, D.-H., Zhou, Y., He, W.-D., Wu, H.-M., & Yu, J. (2019). Influence of rubber ratio and crosslinking agent on mechanical properties, crystallization and rheological behaviors of EPDM/PP thermoplastic elastomer. *International Polymer Processing*, *34*(4), 457-466. https://doi.org/10.3139/217.3817

Xu, J., Cheng, Z., Ke, Y., Yang, C., Wang, B., & Hu, Y. (2025). Combined application of synergists from bittern and bio-based multifunctional modifiers to EPDM rubber composites: processing, fire safety, mechanical and anti-aging properties. *Chemical Engineering Journal*, *515*, 163377. https://doi.org/10.1016/j.cej.2025.163377

Xu, M., Chen, L., & Zong, C. (2025). The effect of rubber and plastic mass ratio on the compatibilized ethylene propylene diene monomer/polypropylene TPV with shape memory behavior. *Journal of Applied Polymer Science*, *142*(2), e56330. https://doi.org/10.1002/app.56330

Yu, F., Long, C., Feng, S., Dong, Z., Liu, X., Li, Y., & Chen, Z.-R. (2025). In-situ grafted ethylene propylene diene monomer (EPDM) rubber multiblock copolymers as compatibilizers for polyethylene (PE) and isotactic polypropylene (iPP) blends. *Polymer*, *317*, 127959. https://doi.org/10.1016/j.polymer.2024.127959

Zhang, C., Wu, J., Teng, F., Su, B., Wang, Y., & Ao, H. (2021). Theoretical and experimental characterization for macro-micro friction behaviors of EPDM rubber. *Polymer Testing*, *99*, 107213. https://doi.org/10.1016/j.polymertesting.2021.107213